Journal of Power Sources 196 (2011) 2841–2847

Contents lists available at ScienceDirect

Journal of Power Sources

journal homepage: www.elsevier.com/locate/jpowsour

A novel sol–gel method based on $FePO_4 \cdot 2H_2O$ to synthesize submicrometer structured $LiFePO_4$/C cathode material

Wenxiu Peng, Lifang Jiao*, Haiyan Gao, Zhan Qi, Qinghong Wang, Hongmei Du, Yuchang Si, Yijing Wang, Huatang Yuan

Institute of New Energy Material Chemistry, Key Laboratory of Advanced Energy Materials Chemistry (MOE), MOE (IRT-0927), Nankai University, Tianjin 300071, PR China

ARTICLE INFO

Article history:
Received 2 August 2010
Received in revised form 7 October 2010
Accepted 21 October 2010
Available online 29 October 2010

Keywords:
Sol–gel method
Lithium iron phosphate
Cathode material
Lithium-ion battery

ABSTRACT

Carbon coated $LiFePO_4$/C cathode material is synthesized with a novel sol–gel method, using cheap $FePO_4 \cdot 2H_2O$ as both iron and phosphorus sources and oxalic acid ($H_2C_2O_4 \cdot 2H_2O$) as both complexant and reductant. In $H_2C_2O_4$ solution, $FePO_4 \cdot 2H_2O$ is very simple to form transparent sols without controlling the pH value. Pure submicrometer structured $LiFePO_4$ crystal is obtained with a particle size ranging from 100 to 500 nm, which is also uniformly coated with a carbon layer, about 2.6 nm in thickness. The as-synthesized $LiFePO_4$/C sample exhibits high initial discharge capacity 160.5 mAh g^{-1} at 0.1 C rate, with a capacity retention of 98.7% after 50th cycle. The material also shows good high-rate discharge performances, about 106 mAh g^{-1} at 10 C rate. The improved electrochemical properties of as-synthesized $LiFePO_4$/C are ascribed to its submicrometer scale particles and low electrochemical impedance. The sol–gel method may be of great interest in the practical application of $LiFePO_4$/C cathode material.

1. Introduction

Since the pioneering work of Goodenough and co-workers in 1997 [1], olivine structured lithium iron phosphate, $LiFePO_4$, has been recognized as a promising cathode material for lithium ion batteries. Compared with other cathode materials, $LiFePO_4$ exhibits the advantages of high theoretical capacity (170 mAh g^{-1}), low cost, nontoxicity, excellent thermal safety, high reversibility and repeatability and so on. But its intrinsic low electronic and lithium ion conductivities hold back the practical application. Many original ideas have been tried to solve these problems, such as coating conductive materials-carbon [2], metal [3], polymer [4] or metal oxide [5] on the particles, doping supervalent cations [6,7] or anion [8] into the olivine structure and, especially, minimizing the particle size [9] with different synthesis methods. These synthesis methods contain solid-state reaction [10], carbon thermal reduction [11], sol–gel [12], co-precipitation [13], microwave processes [14], hydrothermal route [15], solvothermal method [16,17], emulsion drying synthesis [18], vapor deposition [19], spray solution technology [20] and pulsed laser deposition [21] and so on.

Among these synthesis methods, sol–gel is particularly attractive, because all reactants could be homogeneously mixed even at an atomic level, which is favorable to synthesize small pure products and well-distributed particles. In the reported sol–gel methods, water-soluble iron (II)/(III) salts were usually chosen as iron sources such as $FeCl_2$ [22], $Fe(CH_3COO)_2$ [23], $Fe(NO_3)_3$ [24], Fe(III)-citrate [25,26] and so on, but they brought on high synthesis cost, especially for iron (II) salts. There were seldom reports using cheap water-insoluble iron (II)/(III) salts as iron sources with sol–gel methods but being introduced in other synthesis methods. Kang and Ceder1 [27] obtained $LiFePO_4$/C material with the size of about 50 nm by solid-state reaction using $FeC_2O_4 \cdot 2H_2O$ as iron source and it showed good high-rate discharge performances, about 140 mAh g^{-1} at 20 C rate. Wang et al. [28] synthesized $LiFePO_4$/C with the size ranging from 100 to 300 nm from $FePO_4 \cdot 4H_2O$ through a solid–liquid phase reaction using $(NH_4)_2SO_3$ as reducing agent, followed by thermal conversion of intermediate NH_4FePO_4 in $LiCOOCH_3 \cdot 2H_2O$. Huang et al. [29] synthesized $LiFePO_4$/C composite with 100~200 nm in size by a soluble starch sol assisted rheological phase method using nano-$FePO_4$ as the iron source. It also indicated good high-rate discharge performances, about 72 mAh g^{-1} at 30 C rate. Zheng et al. [30] obtained nano $LiFePO_4$/C by heating amorphous $LiFePO_4$/C, which was synthesized through lithiation of $FePO_4 \cdot xH_2O$ by using oxalic acid as reducing agent. It exhibited a discharge capacity of 166 mAh g^{-1} at 0.1 C rate. Sinha et al. [31] prepared $LiFePO_4$/C nanoplates from $FePO_4$ and LiOH by a simple polyol route, and obtained discharge capacities of 160 and 100 mAh g^{-1} at 0.15 and 3.45 C, respectively.

In this paper, we describe a novel sol–gel method using cheap water-insoluble $FePO_4 \cdot 2H_2O$ as both iron and phosphorus sources and oxalic acid as both complexant and reductant to form transparent sols without controlling the pH value, which has not been

* Corresponding author. Tel.: +86 22 23498089; fax: +86 22 23502604.
E-mail address: jiaolf@nankai.edu.cn (L. Jiao).

0378-7753/$ – see front matter © 2010 Elsevier B.V. All rights reserved.
doi:10.1016/j.jpowsour.2010.10.065

reported in the previous paper. The reacting mechanism and electrochemical performances were also investigated. The sol–gel method would be attractive in the commercial application of $LiFePO_4$ cathode material.

2. Experimental

2.1. Preparation of $LiFePO_4$/C

$LiFePO_4$/C material was synthesized with a novel sol–gel method from a stoichiometric mixture of $FePO_4{\cdot}2H_2O$, $LiOH{\cdot}H_2O$ and oxalic acid ($H_2C_2O_4{\cdot}2H_2O$), with glucose as carbon source. These reactants were dissolved into distilled water and strongly stirred at 90 °C until a light green clear sol was formed. Then they were placed into an oven and kept at 90 °C to form xerogel precursors. After being ground, they were pressed into a pellet and preheated at 300 °C for 6 h under Ar atmosphere. After cooled to room temperature, the pellet was ground, pressed into a pellet again and calcined at 600 °C for 6 h in Ar atmosphere. Finally, $LiFePO_4$/C submicrometer-crystal was obtained.

2.2. Characterization of $LiFePO_4$

Thermogravimetric (TG) analysis of the precursor was investigated on a STA904 apparatus in the temperature range from room temperature to 700 °C under Ar flow with a heating rate of 5 °C min^{-1}. X-ray diffraction (XRD) pattern was recorded using a Rigaku D/Max III diffractometer with Cu Kα radiation (λ = 1.5418 Å). The morphology was observed using a Hitachi S-3500N scanning electron microscope (SEM). The inner microstructure was tested with a Tecnai 20 transmission electron microscrope (TEM). The Carbon content was analyzed by a Perkin-Elmer 2400 Series II CHNS/O elemental analyzer.

2.3. Cell assembly

Electrochemical performances of $LiFePO_4$/C were evaluated in Li test cell. Lithium metal was used as anode and Celgard 2320 as separator. The electrolyte was composed of 1 M $LiPF_6$ dissolved in ethylene carbonate (EC), ethylene methyl carbonate (EMC) and dimethyl carbonate (DMC) with a volume ratio of 1:1:1. The cathode material contained $LiFePO_4$ active material, acetylene black and polytetrafluoroethylene (PTFE) with a weight ratio of 80:15:5. The test cells were assembled in an argon-filled dry glove box.

2.4. Electrochemical tests

Galvanostatic charge/discharge measurements were operated on a Land CT2001 automatic battery tester at different current densities in a voltage range of 2.5–4.2 V at 25 °C. Cyclic voltammogram (CV) was recorded with a Zahner-Elektrik IM6e electrochemical workstation in the potential range of 2.5–4.2 V at various scan rates (0.1–2 mV s^{-1}) at 25 °C. Electrochemical impedance spectrum (EIS) was also measured with the same electrochemical workstation in a frequency range of 10 kHz–10 mHz. It is necessary to point out that the electrochemical tests were carried out using active materials with the same weight.

3. Results and discussion

Oxalic acid plays an important role in the preparation of $LiFePO_4$/C submicrometer material with this novel sol–gel method, which acts as both complexant and reductant. The reaction process is described according to the following steps:

$$FePO_4 + 3H_2C_2O_4 \rightarrow H_3Fe(C_2O_4)_3 + H_3PO_4 \quad (1)$$

$$2H_3PO_4 + 2H_3Fe(C_2O_4) + 2LiOH \rightarrow 2LiFePO_4 + 7CO_2 + 5CO + 7H_2O \quad (2)$$

The overall reaction could be expressed as:

$$2FePO_4 + 6H_2C_2O_4 + 2LiOH \rightarrow 2LiFePO_4 + 7CO_2 + 5CO + 7H_2O \quad (3)$$

As the reactants gradually dissolved, reaction (1) takes place and the solution gradually becomes yellow. At last, the yellow solution changes to clear aqua, indicating Fe^{3+} coordinated by oxalic acid. The feasibility of reaction (1) could be explained according to the six equations from (4) to (9).

$$H_2C_2O_4 \leftrightarrow H^+ + [HC_2O_4]^- \quad K_{a1} \quad (4)$$

$$[HC_2O_4]^- \leftrightarrow H^+ + [C_2O_4]^{2-} \quad K_{a2} \quad (5)$$

$$Fe^{3+} + [(C_2O_4)]^{2-} \leftrightarrow [Fe(C_2O_4)]^+ \quad K_1 \quad (6)$$

$$[Fe(C_2O_4)]^+ + [(C_2O_4)]^{2-} \leftrightarrow [Fe(C_2O_4)_2]^- \quad K_2 \quad (7)$$

$$[Fe(C_2O_4)_2]^- + [(C_2O_4)]^{2-} \leftrightarrow [Fe(C_2O_4)_3]^{3-} \quad K_3 \quad (8)$$

$$FePO_4 \leftrightarrow Fe^{3+} + (PO_4)^{3-} \quad K_{sp} \quad (9)$$

In our synthesis process, $H_2C_2O_4$ contains the ionization equilibrium reactions (4) and (5) in aqueous solution. With the gradual dissolution of $H_2C_2O_4$ and the evaporation of distilled water, the increased concentration of $[C_2O_4]^{2-}$ results in the occurrence of the forward reaction of reversible reactions from (6) to (8), which leads to the decrease in the concentration of Fe^{3+} and the dissolution of $FePO_4$ in reversible equation (9).

And the expression of the final concentration of $[Fe(C_2O_4)_3]^{3-}$ could also be calculated based on the reversible reactions (4)–(9):

$$\{[Fe(C_2O_4)_3]^{3-}\} = K_{a1}K_{a2}K_1K_2K_3K_{sp}[H_2C_2O_4]_0{}^3[H^+]_0{}^{-6} \quad (I)$$

where K_{a1} ($\sim 10^{-2}$) and K_{a2} ($\sim 10^{-5}$) are the first and second ionization constant of oxalic acid; K_1 ($\sim 10^{9.4}$), K_2 ($\sim 10^{6.8}$) and K_3 ($\sim 10^4$) are stepwise stability constants of $[Fe(C_2O_4)_3]^{3-}$; K_{sp} ($\sim 10^{-22}$) is the solubility-product constant of $FePO_4$; $[H]_0{}^+$ is the initial concentration of H^+; and $[H_2C_2O_4]_0$ is the initial oxalic acid concentration. According to (I), it is clearly showed that the concentration of $[H_2C_2O_4]_0$ and $[H^+]_0$ is crucial to the formation of $[Fe(C_2O_4)_3]^{3-}$, which could be realized in our synthesis route with two methods: the sufficient mol quantity of $H_2C_2O_4$ and the evaporation of distilled water.

Compared with the previous reported sol–gel methods [32,33], there are some advantages in our synthesis route. The most important is that $FePO_4{\cdot}2H_2O$ powders are very cheap and simple to form transparent sols because of the strong complexation ability of $(C_2O_4)^{2-}$, which reduces the kinds of the reactants and the synthesis cost. But in other sol–gel methods [12,33], the pH value needs being carefully controlled in order to form clear sols, because Fe^{3+} is very inclined to form $Fe(OH)_3$ or $FePO_4$ precipitations in weak acid and strong basic conditions and $LiFePO_4$ could partly dissolve in strong acid. Also, the decomposition product of oxalic acid is a mixture of CO, CO_2 and H_2O, with no contaminated gases released during calcination process. At last, the produced gases would restrain the particles from congregating, which would form small and well-distributed particles.

3.1. Material characterization

Fig. 1 is the TG/DTA curve of the xerogel precursors, at a heating rate of 5 °C min^{-1} from room temperature to 700 °C in Ar atmosphere. The TG curve presents three steps of weight loss and DTA curve displays several corresponding exothermic peaks. Release of physically absorbed and crystallized water occurs below 160 °C,

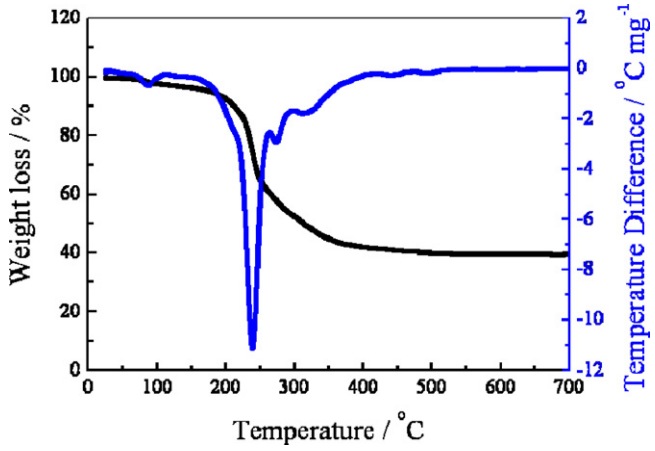

Fig. 1. The TG/DTA curve for the precursor recorded from room temperature to 700 °C at a heating rate of 5 °C min^{-1} in Ar atmosphere.

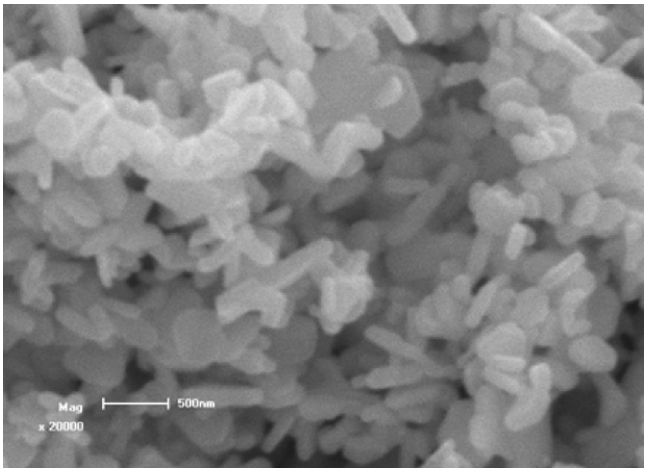

Fig. 4. SEM image of $LiFePO_4$/C material.

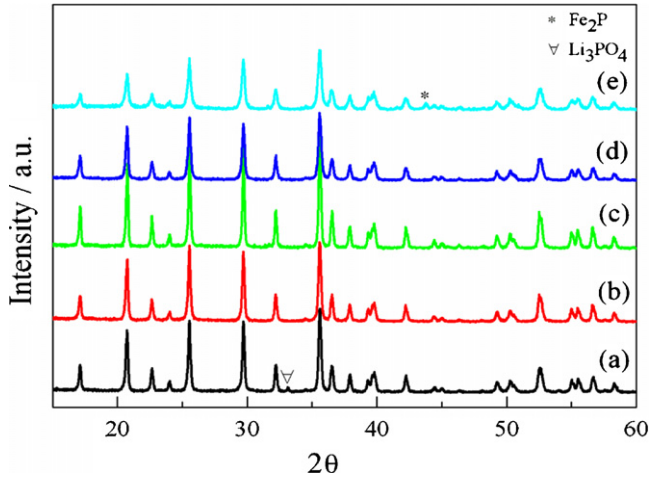

Fig. 2. XRD patterns of $LiFePO_4$/C calcined at (a) 500, (b) 550, (c) 600, (d) 650 and (e) 700 °C.

and there is a small exothermic peak in this temperature range. The main weight loss between 160 and 400 °C can be ascribed to a complicated process including the decomposition of the reactants and glucose, the iron-related redox reaction and so on. So there is a main exothermic peak and several small exothermic peaks in the corresponding DTA curve. The final small weight loss from 400 to 520 °C may correspond to the crystallization of phosphate, and very small exothermic peaks appear in DTA curve. Above 520 °C, there is nearly no weight loss in TG curve and no exothermic peaks in DTA curve, which indicates the complete crystallization of $LiFePO_4$. Therefore, it is possible to calcine the precursor above 520 °C to obtain well-crystallized $LiFePO_4$. In this study, thermal conversion and subsequent crystalline growth of $LiFePO_4$/C material was post-treated by heating at 500, 550, 600, 650 and 700 °C for 12 h.

The XRD patterns of $LiFePO_4$/C materials synthesized from 500 to 700 °C are shown in Fig. 2. On one hand, the main diffraction peaks of the $LiFePO_4$/C samples from 550 to 650 °C are all in good accordance with the standard $LiFePO_4$ crystal (JCPDS 81-1173) – olivine structure indexed by orthorhombic *Pnmb*. Few differences are founded in XRD response among these samples which suggests the crystal growth of $LiFePO_4$ can be achieved at 550 °C (as low as 520 °C analyzed in TG/DTA curve). But the diffraction peaks synthesized at 600 °C are the highest and sharpest, so we choose it as the final calcination temperature. And we perform Rietveld refinement on the XRD pattern (Fig. 3) synthesized at this temperature to obtain the cell parameters (a = 10.333 Å, b = 6.011 Å, c = 4.698 Å), indicating a highly crystalline $LiFePO_4$ phase (JCPDS 81-1173, a = 10.330 Å, b = 6.010 Å, c = 4.692 Å). Because the *Rwp* and *Rp* values are less than 10%, the Rietveld refinement results are reliable. On the other hand, when the temperature is lower than 500 °C or higher than 700 °C, impurity phases such as Li_3PO_4 [6] and Fe_2P [34] appear. No typical diffraction peaks of carbon are found, so carbon yielded from the decomposition of glucose should exist in amorphous form.

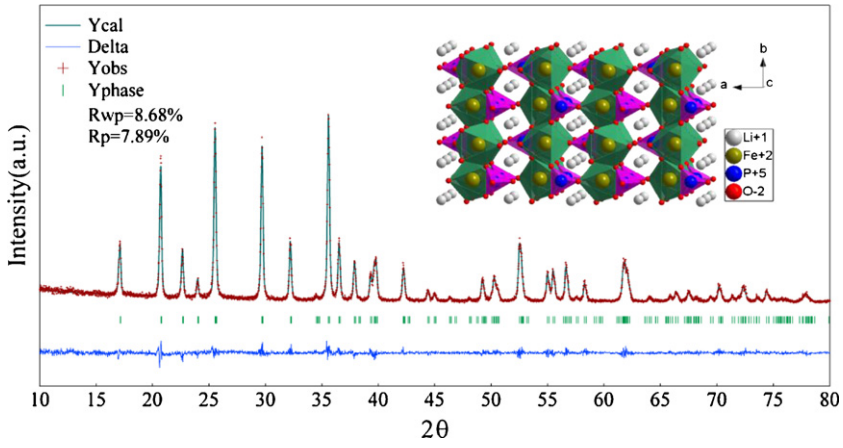

Fig. 3. Rietveld refinement of $LiFePO_4$/C synthesized at 600 °C.

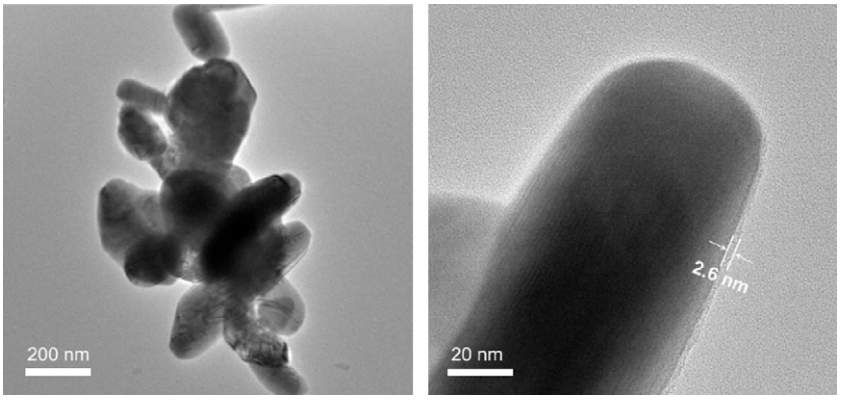

Fig. 5. TEM images of $LiFePO_4$/C material.

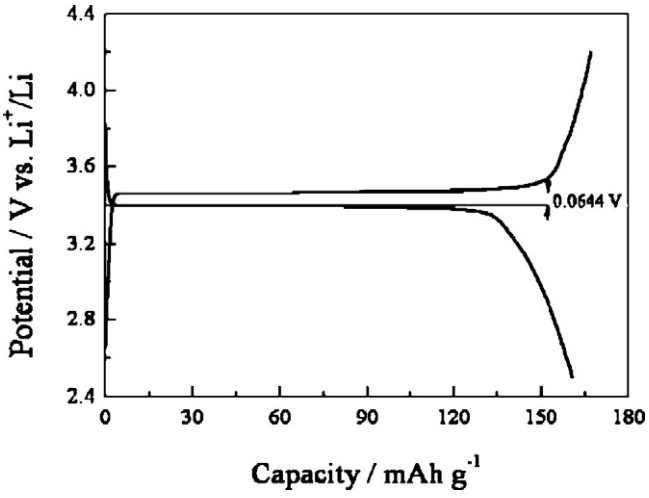

Fig. 6. Initial charge–discharge curves of $LiFePO_4$/C material at 0.1 C rate.

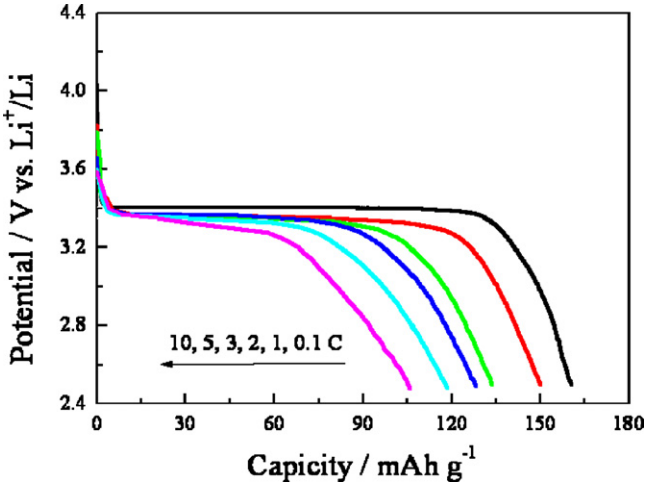

Fig. 7. First discharge curves of $LiFePO_4$/C at different current densities.

Fig. 4 shows the SEM image of the as-synthesized $LiFePO_4$/C composite. Well-distributed submicrometer-size particles are observed. The particle size ranges from 100 to 500 nm. The TEM image (Fig. 5) indicates that the inner $LiFePO_4$ material (black) is uniformly coated with a carbon layer (grey), about 2.6 nm in thickness. The carbon content is about 5.9 wt%, revealed by the elemental analyzer.

3.2. Galvanostatic charge/discharge measurements

The initial charge/discharge curves of the $LiFePO_4$/C sample are shown in Fig. 6, at 0.1 C rate in the voltage range of 2.5–4.2 V at room temperature. The first charge and discharge capacities are 166.9 and 160.5 mAh g^{-1}, which is close to the theoretical capacity (170 mAh g^{-1}). The plateau potential difference is about 0.064 V, which accords well with the previous paper [35] and confirms an excellent electrochemical reversibility. When the current density increases to 1, 2, 3, 5 and 10 C rates, the initial discharge capacities are about 150, 133.7, 128.1, 118.3, 106 mAh g^{-1} (Fig. 7), which indicates good high-rate performances. The rate performances are a little superior to the reported sol gel method [25].

3.3. Cyclic charge/discharge measurements

Fig. 8 displays the cyclic performances of $LiFePO_4$/C sample at 0.1 C rate. After 50 cycles, the discharge capacity maintains 158.2 mAh g^{-1} with a capacity retention of 98.7%, which displays good cyclic stability. And the cyclic curves in every first 20 cycles at 0.1–10 C rates are displayed in Fig. 9. The capacity retentions are 99.1%, 98.8%, 99.6%, 99.4%, 99.7% and 99.2%, respectively. When recovering the former testing current densities, the discharge capacities decrease by no more than 2 mAh g^{-1} in all situations, which indicates good cyclic reversibility.

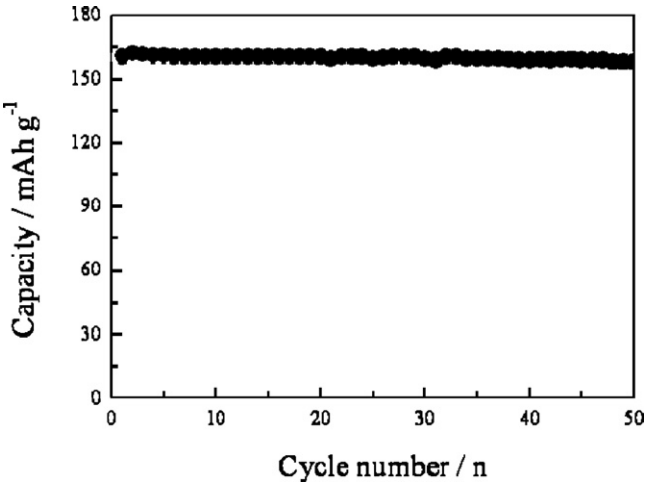

Fig. 8. Cyclic curve of $LiFePO_4$/C material at 0.1 C rate.

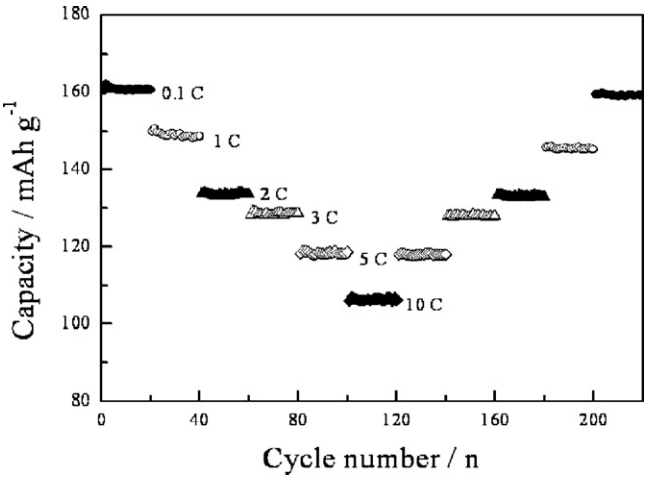

Fig. 9. Cyclic performances of $LiFePO_4$/C at different current densities.

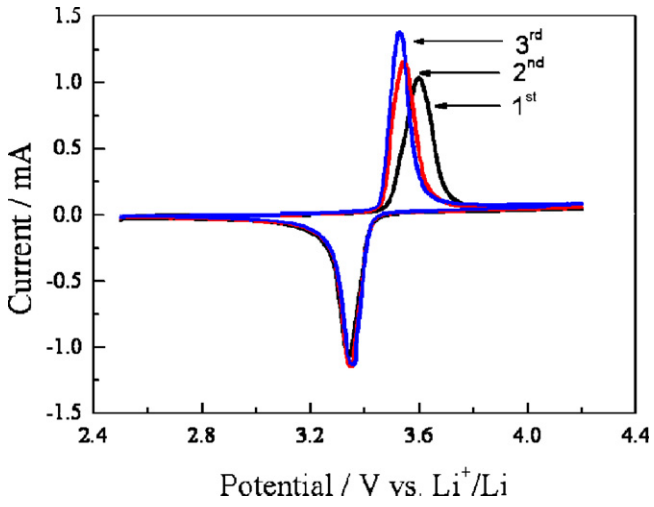

Fig. 10. Cyclic voltammograms of $LiFePO_4$/C at the first three cycles at a scan rate of 0.1 mV s^{-1}.

Table 1
Anodic peak potential locations ($E_{p,a}$) and corresponding cathodic ones ($E_{p,c}$) and potential differences (ΔE) for the CV curve in Fig. 10.

Cycle	$E_{p,a}$, V	$E_{p,c}$, V	ΔE, V
First	3.596	3.340	0.256
Second	3.542	3.348	0.194
Third	3.524	3.356	0.168

3.4. CV measurements

The CV curves of $LiFePO_4$/C sample during the first three cycles are shown in Fig. 10, in the potential range of 2.5–4.2 V at a scan rate of 0.1 mV s^{-1}. There is a pair of redox peaks during each circle, corresponding to the extraction/insertion of lithium ions from/into the bulk. The difference between oxidation and reduction peak potential becomes smaller during cycling (Table 1), indicating good electrochemical reversibility. And the high oxidation/reduction peak current indicates fast lithium-ion diffusion.

The CV curves at different scan rates – 0.1, 0.2, 0.5, 1 and 2 mV s^{-1} are also studied in this paper, shown in Fig. 11. The peak current density significantly increases with the scan rate increasing. The anodic peaks shift to higher potentials and the cathodic ones to lower potentials, which indicates increased kinetic polarization and increased internal resistance [36]. And it is found that the redox peak current density is in direct ratio to $\upsilon^{1/2}$ (Fig. 12), so the final apparent lithium ion diffusivity could be obtained according to the conventional computing formula [37]:

$$I_p = 0.4463 \times 10^{-3} F^{3/2} n^{3/2} A {D_{Li+}}^{1/2} C \upsilon^{1/2} (CR)^{-1/2} \quad \text{(II)}$$

Among (II), I_p is the redox peak current, F is Faraday content, n is the transition number of electrons, A is the contact area, C is the mol concentration of Li^+, D_{Li+} is the final apparent lithium ion diffusivity, υ is the scan rate. The obtained D_{Li+} is at an order of 10^{-14} cm^2 s^{-1} for both charging and discharging electrodes. The results are 4 orders of magnitude as fast as the pure $LiFePO_4$

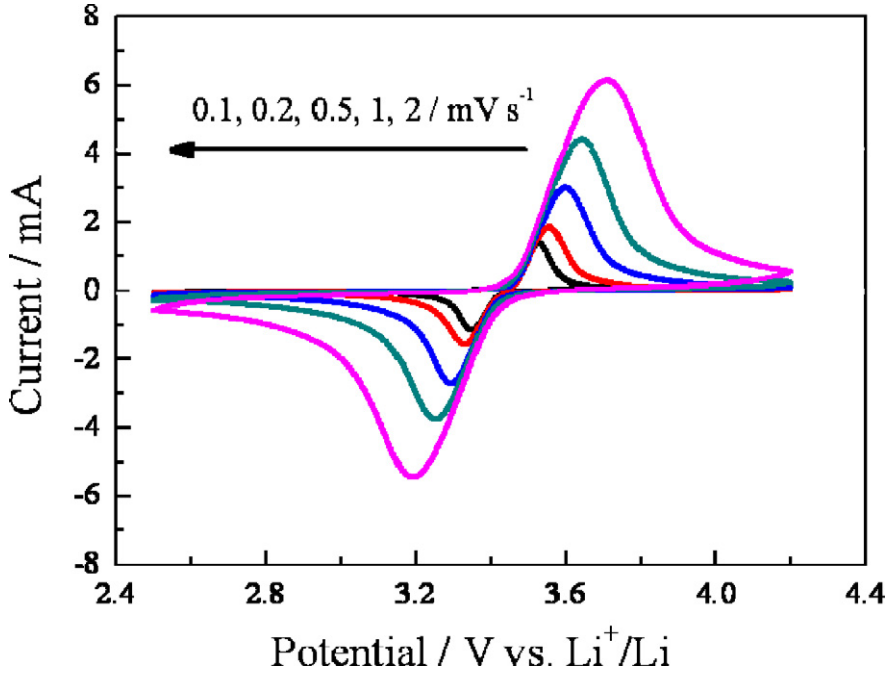

Fig. 11. CV curves of $LiFePO_4$/C at different scan rates.

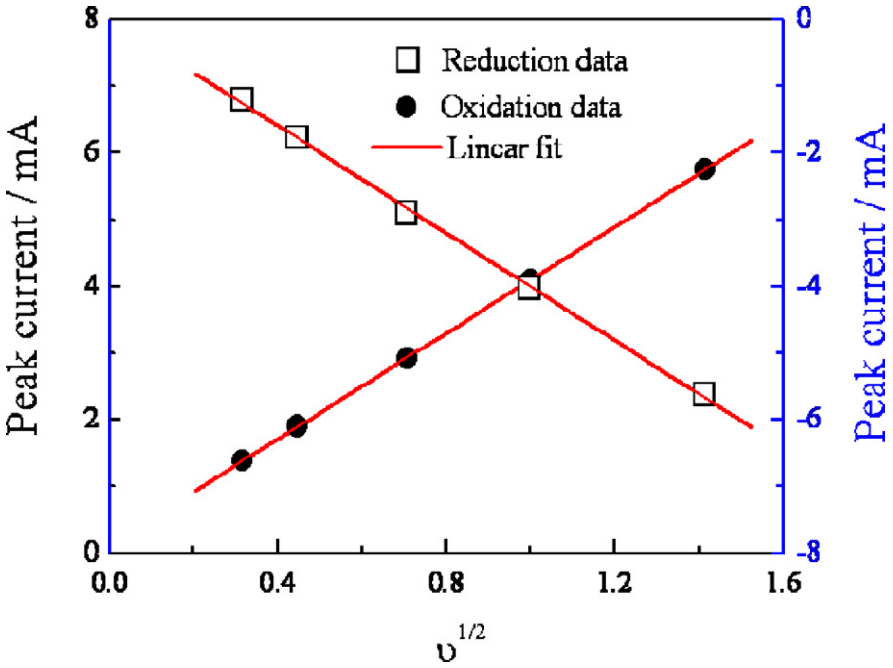

Fig. 12. Variation of redox peak current to scan rate $\upsilon^{1/2}$ for $LiFePO_4$/C material.

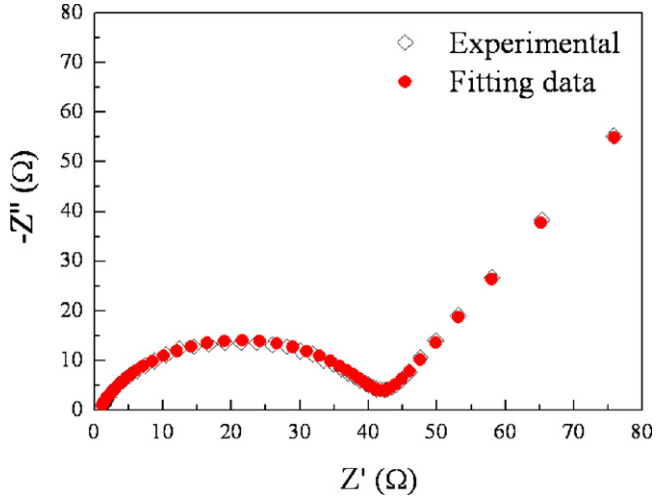

Fig. 13. The Nyquist plot of $LiFePO_4$/C tested at the first discharging potential plateau.

material ($\sim 1.8 \times 10^{-18}$ cm^2 s^{-1}) and are consistent with the previous report of Yu et al. [35], who obtained apparent Li^+ diffusion constants-2.2×10^{-14} and 1.4×10^{-14} cm^2 s^{-1} for charging and discharging $LiFePO_4$ electrodes.

3.5. EIS measurements

EIS is a very important method to investigate the electrochemical resistances, such as the solid electrolyte interface (SEI) film, electrolyte/electrode interface, charge transfer and lithium-ion diffusion resistances. Fig. 13 shows the Nyquist plot of the as synthesized $LiFePO_4$/C material during the first discharging potential plateau. The curve is comprised of one semicircle in high frequency and an inclined line in low frequency. The high-frequency semicircle corresponds to the charge-transfer resistance and the inclined line is related to the diffusion resistance of lithium ion in the bulk. After fitting the experimental data, the charge-transfer and Warburg resistances are as low as 39.05 and 4.79 Ω, respectively, indicating fast electrochemical reaction and lithium diffusion processes. The results are very similar to ferric citrate based sol–gel method reported by Dupre et al. [38], but much lower than solid state technique [10], co-precipitation [39] or hydrothermal method [40]. The lowered electrochemical resistances are attributed to the small particles which results in short lithium-ion diffusion distance and the conductive carbon layer which results in fast electron transfer rate.

4. Conclusions

$LiFePO_4$/C cathode material was synthesized with a novel sol–gel method-cheap $FePO_4 \cdot 2H_2O$ was chosen as both iron and phosphorus sources which could reduce the synthesis cost; cheap $H_2C_2O_4$ was chosen as both reductant and complexant which was able to form transparent and homogeneous sols; in the calcination process, the produced CO and CO_2 gases could prevent the particles from aggregating and growing up which was helpful to synthesize small and well-distributed particles. XRD and SEM demonstrated well-crystallized $LiFePO_4$ material and well-distributed submicrometer-size particles. TEM showed that $LiFePO_4$ material was uniformly coated with a carbon layer, with about 2.6 nm in thickness. The initial discharge capacity of the obtained $LiFePO_4$ material was as high as 160, 150, 134, 128, 118 and 106 mAh g^{-1} at 0.1, 1, 2, 3, 5 and 10 C rates, respectively, in the potential range of 2.5–4.2 V. The cyclic performances were good-only 2.4 mAh g^{-1} decreased after 50 cycles at 0.1 C rate, with a capacity retention of 98.7%. The improvement of the electrochemical performances could be attributed to fast electronic conductivity and lithium-ion diffusivity resulting from the carbon-coated submicrometer-size particles.

Acknowledgements

This work was supported by NSFC (20801059, 21073100), 973 program (2010CB631303) and TSTC (10JCYBJC08000).

References

[1] A.K. Padhi, K.S. Nanjundaswamy, J.B. Goodenough, J. Electrochem. Soc. 144 (1997) 1188.
[2] Y. Hu, M.M. Doeff, R. Kostecki, R. Finones, J. Electrochem. Soc. 1518 (2004) A1279.
[3] F. Croce, A.D. Epifanio, J. Hassoun, A. Deptula, T. Olczac, B. Scrosati, Electrochem. Solid-State Lett. 5 (2002) A47.
[4] Y.H. Huang, J.B. Goodenough, Chem. Mater. 20 (2008) 7237.
[5] Y.-S. Hu, Y.-G. Guo, R. Dominko, M. Gaberscek, J. Jamnik, J. Maier, Adv. Mater. 19 (2007) 1963.
[6] P.S. Herle, B. Ellis, N. Coombs, L.F. Nazar, Nat. Mater. 3 (2004) 147.
[7] M.R. Yang, W.H. Ke, J. Electrochem. Soc. 155 (2008) A729.
[8] R. Amin, C.T. Lin, J.B. Peng, K. Weichert, T. Acarturk, U. Starke, J. Maier, Adv. Funct. Mater. 19 (2009) 1697.
[9] K.S. Park, K.T. Kang, S.B. Lee, G.Y. Kim, Y.J. Park, H.G. Kim, Mater. Res. Bull. 39 (2004) 1803.
[10] H. Liu, C. Li, H.P. Zhang, L.J. Fu, Y.P. Wu, H.Q. Wu, J. Power Sources 159 (2006) 717.
[11] J. Barker, M.Y. Saidi, J.L. Sowyer, Electrochem. Solid-State Lett. 6 (2003) A53.
[12] Y.Q. Hu, M.M. Doeff, R. Kostecki, R. Finonesa, J. Electrochem. Soc. 151 (2004) A1279.
[13] Y. Ding, Y. Jiang, F. Xu, J. Yin, H. Ren, Q. Zhuo, Z. Long, P. Zhang, Electrochem. Commun. 12 (2010) 10.
[14] K.S. Park, J.T. Son, H.T. Chung, S.J. Kim, C.H. Lee, H.G. Kim, Electrochem. Commun. 5 (2003) 839.
[15] J.F. Qian, M. Zhou, Y.L. Cao, X.P. Ai, H.X. Yang, J. Phys. Chem. C 114 (2010) 3477.
[16] Y.H. Huang, K.S. Park, J.B. Goodenough, J. Electrochem. Soc. 153 (2006) A2282.
[17] D. Rangappa, K. Sone, T. Kudo, I. Honma, J. Powder Sources 195 (2010) 6167.
[18] T.-H. Cho, H.-T. Chung, J. Power Sources 133 (2004) 272.
[19] I. Belharouak, C. Johnson, K. Amine, Electrochem. Commun. 7 (2005) 983.
[20] K. Konstantinov, S. Bewlay, G.X. Wang, M. Lindsay, J.Z. Wang, Electrochim. Acta 50 (2004) 421.
[21] V. Palomares, I.R. de Larramendi, J. Alonso, M. Bengoechea, A. Goni, O. Miguel, T. Rojo, Appl. Surf. Sci. 256 (2010) 2563.
[22] D. Choi, P.N. Kumta, J. Power Sources 163 (2007) 1064.
[23] S.B. Lee, S.H. Cho, S.J. Cho, G.J. Park, S.H. Park, Y.S. Lee, Electrochem. Commun. 10 (2008) 1219.
[24] Y.Y. Liu, C.B. Cao, J. Li, Electrochim. Acta 55 (2010) 3921.
[25] S. Beninati, L. Damen, M. Mastragostino, J. Power Sources 194 (2009) 1094.
[26] C. Arbizzani, S. Beninati, M. Mastragostino, J. Appl. Electrochem. 40 (2010) 7.
[27] B. Kang, G. Ceder1, Nature 458 (2009) 190.
[28] Y.Q. Wang, J.L. Wang, J. Yang, Y. Nuli, Adv. Funct. Mater. 16 (2006) 2135.
[29] Y.H. Huang, H.B. Ren, S.Y. Yin, Y.H. Wang, Z.H. Peng, Y.H. Zhou, J. Power Sources 195 (2010) 610.
[30] J.C. Zheng, X.H. Li, Z.X. Wang, H.J. Guo, S.Y. Zhou, J. Power Sources 184 (2008) 574.
[31] N.N. Sinha, N. Munichandraiah, J. Electrochem. Soc. 157 (7) (2010) A824.
[32] D. Choi, P.N. Kumt, J. Power Sources 163 (2007) 1064.
[33] Z.H. Xu, L. Xu, Q.Y. Lai, X.Y. Ji, Mater. Res. Bull. 42 (2007) 883.
[34] S. Franger, F. Cras, C. Bourbon, H. Rouault, Electrochem. Solid-State Lett. 5 (2002) 231.
[35] D.Y.W. Yu, C. Fietzek, W. Weydanz, K. Donoue, T. Inoue, H. Kurokawa, S. Fujitani, J. Electrochem. Soc. 154 (4) (2007) A253.
[36] K.-L. Lee, J.-Y. Jung, S.-W. Lee, H.-S. Moon, J.-W. Park, J. Power Sources 130 (2004) 241.
[37] A.J. Bard, L.R. Faulkner, Electrochemical Methods, John Wiley & Sons Inc., New York, 1980, p. 213.
[38] N. Dupre, J.-F. Martin, J. Degryse, V. Fernandez, P. Soudan, D. Guyomard, J. Power Sources 195 (2010) 7415.
[39] Y.Y. Liu, C.B. Cao, Electrochim. Acta 55 (2010) 4694.
[40] J.L. Liu, R.R. Jiang, X.Y. Wang, T. Huang, A.S. Yu, J. Power Sources 194 (2009) 536.